Shewanella oneidensis MR-1 in situ biosynthesis of Ag nanoparticles on TiO_2 nanotubes with enhanced photocatalytic performance

Xiaojie Song[1], *Fan Yang*[2] ✉, *Xiufang Wang*[1], *Kehua Zhang*[1]

[1]*School of Materials and Chemical Engineering, Anhui Jianzhu University, Hefei 230601, People's Republic of China*
[2]*Department of Chemistry, Anhui Medical University, Hefei 230026, People's Republic of China*
✉ *E-mail: fyang99@126.com*

Published in Micro & Nano Letters; Received on 15th May 2020; Revised on 2nd July 2020; Accepted on 20th July 2020

Biogenetic nanocomposites research provides valuable methods for the green synthesis of nanomaterials. As a dissimilatory metal-reducing bacterium, *Shewanella oneidensis* MR-1 is used to reduce Ag^+ to Ag nanoparticles (Ag NPs) (diameter about 10 nm) under anaerobic conditions, resulting in the in-situ formation of Ag NPs immobilised on TiO_2 nanotubes (TNTs) (Ag/TNTs nanocomposites). The loading amount of Ag nanocrystals on the TNT surface can be controlled easily through adjusting the $AgNO_3$ concentration and further influence visible-light absorption efficiency of Ag/TNTs nanocomposites by decreasing the Ag loading amount. Ag/TNTs nanocomposites show superior photocatalytic efficiency under simulated sunlight than single TiO_2 nanomaterials. Moreover, the photocatalytic capacity of Ag/TNTs nanocomposites synergistic by *S. oneidensis* MR-1 is further enhanced and the degradation ratio of methylene blue reaches 92.3% within 30 min which attributed to a synergistic effect.

1. Introduction: Nowadays, *Shewanella oneidensis* widely distributed in the environment is intensively studied for the preparation of nanomaterials due to its considerable reductive capacity [1]. As Gram-negative bacteria are widely distributed in nature, *S. oneidensis* MR-1 can synthesise nanomaterials by transferring electrons generated by its metabolism through anaerobic respiration. The role of *S. oneidensis* MR-1 in the respiratory pathway is very prominent, and it is not necessary to express specific degradation to release the electrons extracellularly so that *S. oneidensis* MR-1 can not only mediate the synthesis of nanomaterials but also synergise nanocomposites to exhibit more excellent catalytic degradation ability for pollutants and significantly improve catalytic degradation efficiency [2].

TiO_2 nanotubes (TNTs) have been regarded as promising candidates as photocatalysts due to the large surface-to-volume ratio, rich activity sites, and direct pathways for charge transport, which make them have better photocatalytic efficiency than traditional TiO_2 nanoparticles (NPs) [3, 4]. However, it can utilise only 5% of total solar energy irradiating because of its wide band gap and exhibit a high-recombination rate of photo-generated electron/hole pairs, which restrict the application of TNTs in photocatalysis [5, 6]. Synthesising heterostructures on the surface of TNTs can produce a built-in electrical potential and reduce the recombination of electron–hole pairs thereby improving photocatalytic performance [7]. Recently, the noble metal/semiconductor heterojunctions, such as Au/TiO_2, Pt/TNT, Pd/TiO_2, and Ag/WO_3 are valuable options [8–10]. Among the noble metals, Ag is particularly attractive because of its much lower cost and application in catalysis, which can reduce the band gap and increase the use of visible light [11, 12]. In terms of environment, the decrease of Ag loading on TiO2 reduces the pollutant degradation efficiency as well as COD removal. Also, this decrease has a slight effect on solution toxicity [13]. The Ag-doped TiO_2 photocatalytic process increases the overall removal efficiencies to 98, and 96% of TOC and COD, respectively [14].

Traditional strategies of synthesis of nanocomposites including sol–gel, chemical reduction, and ultraviolet (UV) irradiation are generally accompanied by rigorous synthetic conditions, toxic reducer, or high consumption of energy [15, 16]. The microbial approach can synthesise the nanocomposites with mild conditions and few chemicals are used in the process. Nowadays, there are some green synthesis approaches for metal [17–19] or metal oxide [20] NPs using natural extracts. Currently, *S. oneidensis* MR-1 is rarely reported for synthesising composites and it is only used to synthesise single nanomaterials such as numerous metals [21–23] and metal sulphide [24]. However, composite materials have better performance, here we synthesise nanocomposites using *S. oneidensis* MR-1.

In this study, Ag NPs were in-situ synthesised on TNTs by *S. oneidensis* MR-1. The photocatalytic activity was researched according to the degradation capability for methylene blue (MB). This process rarely adds chemical reagents, avoiding secondary pollution to the environment. Owing to the wide distribution of the microbial sources and environmental friendliness, the method has attracted much attention. It also provides a new idea for the combination of biological means with chemical methods to complete environmental restoration.

2. Experimental

2.1. Materials: Anatase TiO_2 powder (99.8%, about 25 nm in diameter) was purchased from Aladdin Chemistry (Shanghai, China). All chemicals were analytically pure and used without further purification. $AgNO_3$ dissolved in a modified basal mineral medium (MBMM) to form $AgNO_3$ solution and MBMM was prepared using 20 mM *N*-(2-hydroxyethyl) piperazine-*N*′-2-ethanesulphonic acid and 10 ml stock solution with trace elements in each litre with pH adjusted to 7 using NaOH solution. The detailed formulation of the trace elements could be found in our previous article [2].

S. oneidensis MR-1 was inoculated in serum bottles overnight in Luria–Bertani (LB) medium which contained 100 ml LB medium at 30 °C with shaking (150 rpm) for 24 h. Then the bacteria were collected by centrifugation (6000 rpm) for 20 min and washed with MBMM for three times under aseptic conditions.

2.2. Preparation of TNTs: TNTs were also synthesised in accordance with the process that we published in our previous article [2].

2.3. Synthesis of Ag/TNTs nanocomposites: A total of 1 wt% sodium dodecyl benzene sulphonate (SDS) was prepared in 25 ml of MBMM, and then added a certain quantity of TNTs and

300 mg of polyvinylpyrrolidone with stirring for 4 h at room temperature. Then, $AgNO_3$ was added to the TNTs dispersed solution.

To remove dissolved O_2, the sterilised MBMM was passed with N_2 for 10 min, and then injected with 2 ml of the above silver nitrate/TNTs dispersed solution using a sterile syringe. Subsequently, the collected *S. oneidensis* MR-1 was inoculated in the serum vial getting an initial concentration of 5×0^6 colony-forming units (CFU)/ml. Serum vials were cultured at 30 °C 150 rpm shaker for 120 h. Finally, the product mixture was first centrifuged (5000 rpm) for 20 min to remove the bacteria, then harvested by high-speed centrifugation (10,000 rpm) for 20 min. The product was washed twice with deionised water and dried at 60 °C for 24 h. Different kinds of Ag/TNTs nanocomposites with mass percentages of Ag (5, 10, and 20 wt%) were synthesised.

2.4. Characterisation: The morphologies of the as-prepared materials were observed with energy dispersive X-ray (EDX) analysis and TEM (JEM-2010, Japan). XRD (Rigaku Corp., SmartLab 9KW, Japan) spectra were performed using a Bruker D8-Advance X-ray diffractometer with Cu Kα source ($\lambda = 1.54178$ Å). X-ray photoelectron spectroscopy (XPS, Thermo Fisher, ESCALAB 250Xi, USA) was performed to determine the valence states of the various elements in the nanocomposite. The optical absorption of the TNTs and Ag/TNTs nanocomposites was characterised using the ultraviolet–visible (UV–vis) diffuse reflectance spectroscopy (DRS, Hitachi, U-4100, Japan).

2.5. Photocatalytic activity: To examine the photocatalytic activity of the Ag/TNTs nanocomposites, MB solution was degraded at ambient temperature and pressure under a 300 W iodine–tungsten lamp chosen to simulate a sunlight source with a wavelength range from 350 to 1000 nm. The distance of the lamp relative to the solution is 20 cm and is fixed during the whole experiment.

Then 25 mg photocatalyst was dispersed in 50 ml 40 mg/l MB solution with magnetic stirring for 1 h in the dark to reach the adsorption equilibrium. Sampling was performed at regular intervals, the MB concentration was analysed at 664 nm using a UV–vis spectrophotometer. The photocatalytic activities of different photocatalysts were determined under the same conditions (The amount of photocatalyst and the volume of the dye solution were kept constant.).

3. Results and discussion

3.1. Morphological analysis: The morphology of TNTs, Ag/TNTs nanocomposites, and *S. oneidensis* MR-1 is shown in Fig. 1. In Fig. 1*a*, the as-prepared TNTs, which are shown have a typical tubular structure with a uniform outer diameter of about 10 nm and a length of 100–150 nm. The formation mechanism of TNTs is described in our previous article [2].

As shown in Fig. 1*b*, Ag NPs with a diameter of about 15 nm are-prepared on the TNTs. Fig. 1*c* shows the forming situation of Ag/TNTs nanocomposites using *S. oneidensis* MR-1. A lot of TNTs are fixed on the cell wall of *S. oneidensis* MR-1. Some TNTs' surface is blank, but a certain amount of Ag NPs is synthesised on the other nanotubes. During the synthesis process, electrons are generated from *S. oneidensis* MR-1 metabolic reaction and transmitted from the cytoplasmic membrane to the extracellular TNTs through the anaerobic respiratory pathway constructed with the MtrA–MtrB–MtrC gene cluster in *S. oneidensis* MR-1 [25]. Since SDS is an anionic surfactant, Ag^+ ions can be easily attracted to the surface of the TNTs and accept the electrons to form Ag NPs.

The high-resolution TEM (HRTEM) result (Fig. 1*d*) of the Ag/TNTs nanocomposites demonstrates the interface region between Ag NPs and TNTs. The lattice fringe spacing between two adjacent crystal planes is 0.35 nm, which corresponds to the

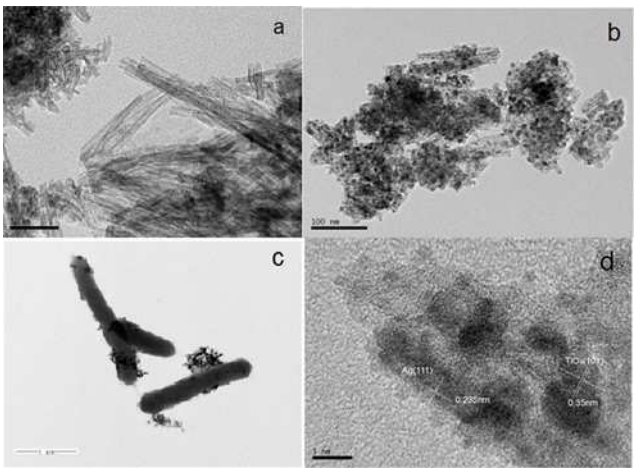

Fig. 1 *Morphological analysis of TNTs, Ag/TNTs nanocomposites, and S. oneidensis MR-1*
a TEM image of TNTs
b TEM image of Ag/TNTs nanocomposites
c TEM image of Ag/TNTs nanocomposites and *S. oneidensis* MR-1
d HRTEM image of Ag/TNTs nanocomposites

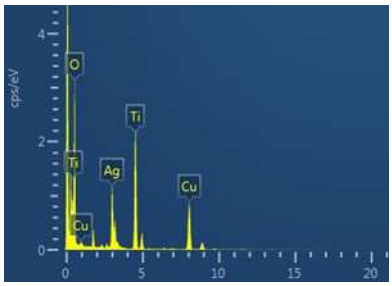

Fig. 2 *EDX image of Ag/TNTs nanocomposites*

(101) lattice planes of anatase. The lattice fringe spacing of 0.235 nm is attributed to the (111) lattice planes of Ag (0) [26].

3.2. EDX analysis: The EDX image (Fig. 2) proves the presence of the three elements, O, Ti and Ag come from TNTs and Ag NPs (Cu comes from copper mesh), which confirms the successful synthesis of Ag/TNTs nanocomposites.

3.3. XRD analysis: Fig. 3 shows the XRD results of TNTs and Ag/TNTs nanocomposites. The diffraction peaks of 2θ values of 25.4°, 32.5°, and 49.8° correspond to the (110), (020), and (022) planes of anatase phase TiO_2 (JCPDS No. 21-1236). Besides, the diffraction peaks at 2θ values of 38.7°, 44.7°, 65.1°, and 77.9° can be associated with the (111), (200), (220), and (311) crystal faces of the face-centred cubic crystalline silver (JCPDS 36-1451). The results imply that Ag/TNTs nanocomposites are formed successfully.

3.4. XPS analysis: The XPS is carried out to confirm the structure of Ag/TNTs nanocomposites. The C, O, Ti, and Ag elements can be found in Fig. 4*a*. The high-resolution O 1s XPS curve can be fitted into three peaks at 530.4, 532.4, and 533.2 eV (Fig. 4*b*), which are assigned to Ti–O, C–O, and C=O, respectively. As shown in Fig. 4*c*, the high-resolution Ag 3d XPS spectrum has two peaks at 368.2 and 374.28 eV, belonging to the Ag $3d_{5/2}$ and Ag $3d_{3/2}$ orbits, respectively.

The spin–orbit splitting of the Ag 3d energy level with a value of 6.1 eV confirms that the Ag element is presented as Ag^0 in the Ag/TNT NPs [27]. Two binding energies at 464.78 and

doi: 10.1049/mnl.2020.0285

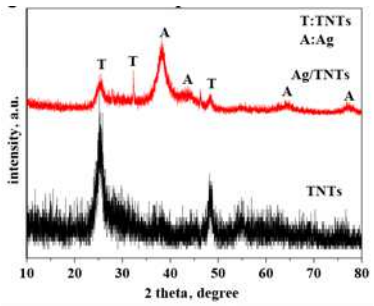

Fig. 3 *XRD patterns of Ag/TNTs nanocomposites*

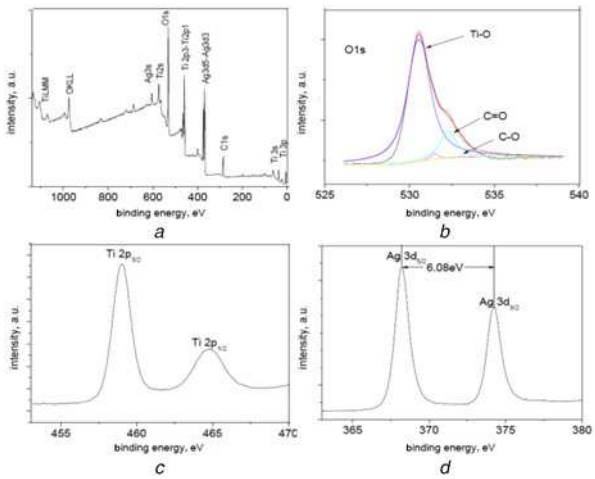

Fig. 4 *XPS analysis*
a XPS spectra of Ag/TNTs nanocomposites: survey scan spectrum
b High-resolution spectra of C 1s
c High-resolution spectra of Ti 2p
d High-resolution spectra of Ag 3d

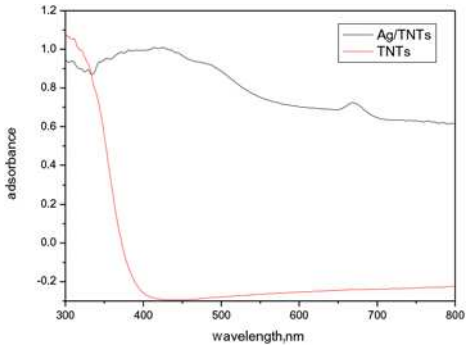

Fig. 5 *UV–Vis DRS of TNTs and Ag/TNTs nanocomposites*

459.02 eV are ascribed to the Ti $2p_{1/2}$ and Ti $2p_{3/2}$ orbits (Fig. 4*d*), respectively, and the peak at 459.02 eV is attributed to the Ti^{4+} in TiO_2 [28]. The binding energy shift of Ag 3d and Ti 2p proves that some electrons may be transferred from TNTs to Ag^0 owing to the strong interaction between Ag and TNTs.

3.5. DRS analysis: The Ag/TNTs nanocomposites show an absorption region of 330–600 m is observed in the visible-light region compared with TNTs (Fig. 5).

It can be attributed to the fact that Ag NPs increase the absorption of TNTs in the visible-light range. Therefore, doping with a transition metal ion such as silver is an effective method for a visible-light response.

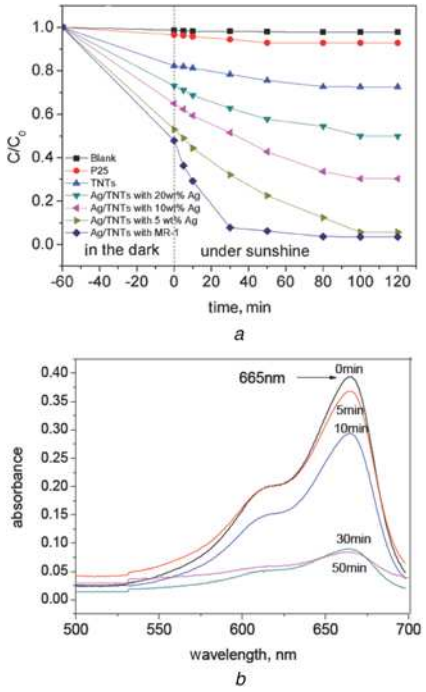

Fig. 6 *Photocatalytic activity results of different catalysts for MB under simulated sunlight*
a Photocatalytic degradation of MB by photocatalysts and Ag/TNTs nanocomposites (5 wt% of Ag) assisted by *S. oneidensis* MR-1 (5×10^6 CFU/ml)
b Absorbance curves of MB in the photocatalysis process by Ag/TNTs nanocomposites (5 wt% of Ag) assisted by *S. oneidensis* MR-1 (5×10^6 CFU/ml)

3.6. Photocatalytic results and mechanism: Photocatalytic activities of different catalysts for MB under simulated sunlight are tested, and results are obtained by measuring the concentration of residual MB and listed in Fig. 6.

As shown in Fig. 6*a*, the photocatalytic capacity of TNTs is superior to P25 because of the larger surface area with a better adsorption capacity. As compared with TNTs, Ag/TNTs nanocomposites show superior photocatalytic performance. The Ag/TNTs with Ag 5 wt% exhibited the best photocatalytic capacity. Through 80 min irradiation, the degradation ratio of MB reaches 87.7%. Based on the surface plasmon resonance mechanism [11, 29], when metal NPs adsorb photons, great electric fields form on the surfaces of nanocomposites. This local electric field not only promotes the generation of photo-induced charges locally in TiO_2 but also reduces the band gap of TiO_2 which lets TiO_2 to make use of visible light. With the utilisation of visible light, more light-excited electrons and holes are generated. The heterogeneous structure of Ag/TNTs nanocomposites promotes the transfer of electrons and the separation of electrons and holes, and the Schottky barrier between TNTs and Ag NPs reduces the recombination of electron–holes. The holes on the surface of TNT react with hydroxyl ions in solution to form hydroxyl radicals ($^{\bullet}OH$) and electrons react with dissolved O_2 to form superoxide anion ($O_2^{\bullet -}$), and superoxide anion ($O_2^{\bullet -}$) can also transform to hydroxyl radicals ($^{\bullet}OH$) through a series of steps [30] as shown in Fig. 7. Both hydroxyl radicals ($^{\bullet}OH$) and superoxide anion ($O_2^{\bullet -}$) can act as an oxidant with strong oxidising for degradation of dyes. All of these result in higher photocatalysis efficiency of Ag/TNTs than TNTs (Fig. 7).

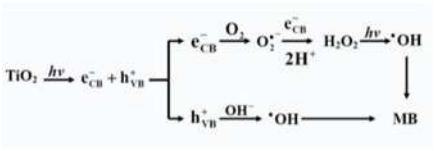

Fig. 7 *Formation of hydroxyl radicals and degradation of MB*

Moreover, the degradation ratio of MB by Ag/TNTs synergistic with *S. oneidensis* MR-1 can be further increased to 92.3% within 30 min. Fig. 6*b* shows the absorbance curves of MB by Ag/TNTs nanocomposites (5 wt% of Ag) synergistic by *S. oneidensis* MR-1. The absorbance value with the maximum wavelength (664 nm) of MB decreases apparently at 30 min in the photocatalysis process.

As an excellent electron donor, *S. oneidensis* MR-1 can release a number of electrons, but it does not show well degradation capacity alone for dye. A possible reason is the lager redox potential between *S. oneidensis* MR-1 and dyes which restrict electrons transfer from *S. oneidensis* MR-1 to dyes. Through the addition of metal NPs or nanocomposites [31–33], it acts as an electrons relay to change electrons transfer step. When electrons transfer from *S. oneidensis* MR-1 to dyes through Ag/TNTs nanocomposites, this change of reaction step presents a decrease of activation energy of the reaction between *S. oneidensis* MR-1 and dye, thereby improve the reaction rate of dye degradation. At the same time, because of the excellent change transfer capacity, adsorption, and stability of TNTs, electrons on the surface of TNTs also can react with adsorbed O_2 to form superoxide anion ($O_2^{\bullet -}$) and hydroxyl radicals ($^{\bullet}OH$) which also can degrade dyes. The presence of *S. oneidensis* MR-1 provides more electrons which not only transfer to dye through Ag/TNTs nanocomposites but also transform to superoxide anion ($O_2^{\bullet -}$) and hydroxyl radicals ($^{\bullet}OH$) on the surface of Ag/TNTs nanocomposites. These changes make Ag/TNTs nanocomposites play more roles in catalytic degradation of dye, so Ag/TNTs nanocomposites assisted with *S. oneidensis* MR-1 show better catalytic degradation capacity than alone Ag/TNTs nanocomposites.

The degradation ratio of MB by Ag/TNTs nanocomposites assisted by *S. oneidensis* MR-1 (5×10^6 CFU/ml) can be further enhanced to 92.3% in 30 min which was demonstrated in Fig. 3*a*. Here, the role of *S. oneidensis* MR-1 is not only used as a metal reducer but also as a model organism for microbial degradation of organics, which has been reported in the previously published article [34]. Electrons produced by organic carbon oxidation in the cell are transmitted via a breathing passage constituted by cytochrome proteins to extracellular electron acceptors [35]. Owing to the superior conductivity, TNTs can change the electrons flow from *S. oneidensis* MR-1 to generate $^{\bullet}OH$. On the one hand, the charge density of the surface of TNTs is increased which promotes the production of $^{\bullet}OH$. At the same time, the adsorption capacity of TNTs is utilised to adsorb MB to the surface of TNTs, which increases the efficiency of MB degradation by light and thus establishes a connection between MB and *S. oneidensis* MR-1. However, excess Ag NPs can fabricate the recombination centre of photo-generated holes and electrons, which lowers the photocatalytic activity. The photocatalysis mechanism of Ag/TNTs nanocomposites and the synergistic effect of *S. oneidensis* MR-1 are shown in Fig. 8.

The reusability of Ag/TNTs nanocomposites is evaluated, and a cyclic experiment is performed. After completion of one catalytic reduction cycle, the intermixture is centrifuged, and a fresh batch of MB is added. As shown in Fig. 9, the catalyst can be successfully recycled and reused for no more than four cycles. After three cycles, the conversion of MB reaches 65.5%, thus, the Ag/TNTs nanocomposites present relatively high reusability for catalytic reduction of MB.

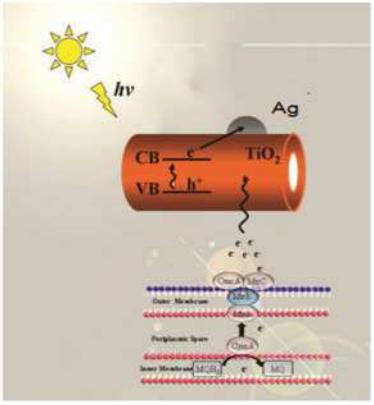

Fig. 8 *Schematic diagram of the mechanism of photocatalytic activity for MB by Ag/TNTs nanocomposites and the synergistic effect of S. oneidensis MR-1*

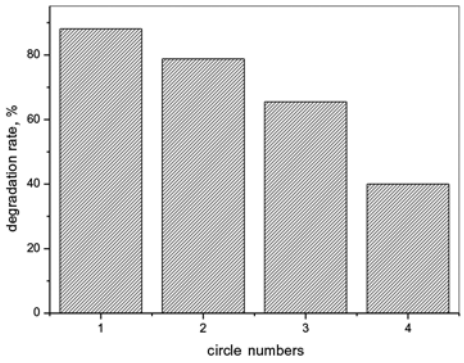

Fig. 9 *Reusability of the Ag/TNTs nanocomposites as a catalyst for the reduction of MB*

4. Conclusions: A facile biosynthesis method under benign conditions assisted by *S. oneidensis* MR-1 is applied for in-situ preparation of Ag/TNTs nanocomposites. Uniform spherical Ag NPs with about 15 nm diameter are prepared on TNTs using *S. oneidensis* MR-1, in which electrons are generated and transmitted through breathing passages to the surface of TNTs and used to form Ag^0. Ag/TNTs nanocomposites display improved photocatalytic efficiency compared to single TNTs and P25 under simulated sunlight in the degradation of MB. The degradation ratio of MB can be further enhanced to 92.3% after 30 min by Ag/TNTs nanocomposites synergistic with *S. oneidensis* MR-1. Such a promising bacterially-based synthesis procedure may have potential valuable inspirations not only for green synthesis of nanocomposites but for efficient contaminant biodegradation.

5. Acknowledgments: This work was supported by the Key Project of Anhui Natural Science Research Fund (grant no. KJ2019A0773) and the project of PhD Research Fund (grant no. 2019QDZ23).

6 References

[1] Heidelberg J.F., Paulsen I.T., Nelson K.E., *ET AL.*: 'Genome sequence of the dissimilatory metal ion-reducing bacterium *Shewanella oneidensis*', *Nat. Biotechnol.*, 2002, **20**, pp. 1118–1123

[2] Song X.J., Shi X.Y., Yang M.: 'Dual application of *Shewanella oneidensis* MR-1 in green biosynthesis of Pd nanoparticles supported on TiO_2 nanotubes and assisted photocatalytic degradation of methylene blue', *IET Nanobiotechnol.*, 2018, **12**, pp. 441–445

[3] Wang Q.Y., Sun C.C., Liu Z.Y., *ET AL.*: 'Ultrasound-assisted successive ionic layer adsorption and reaction synthesis of Cu_2O cubes

doi: 10.1049/mnl.2020.0285

sensitized TiO_2 nanotube arrays for the enhanced photoelectrochemical performance', *Mater. Res. Bull.*, 2019, **111**, pp. 277–283
[4] Abdelnasser S., Park G., Han H., *ET AL.*: 'Enhanced photocatalytic performance of poly(3,4-ethylenedioxythiophene)-coated TiO_2 nanotube electrodes', *Synthetic Met.*, 2019, **251**, pp. 120–126
[5] Huang K.C., Chien S.H.: 'Improved visible-light-driven photocatalytic activity of rutile/titania-nanotube composites prepared by microwave-assisted hydrothermal process', *Appl. Catal. B, Environ.*, 2013, **140**, pp. 283–288
[6] Zhang M., Wu J., Hou J., *ET AL.*: 'Molybdenum and nitrogen Co-doped titanium dioxide nanotube arrays with enhanced visible light photocatalytic activity', *Sci. Adv. Mater.*, 2013, **5**, pp. 535–541
[7] Gomathi D.L., Kavitha R.: 'A review on plasmonic metal TiO_2 composite for generation, trapping, storing and dynamic vectorial transfer of photogenerated electrons across the Schottky junction in a photocatalytic system', *Appl. Surf. Sci.*, 2016, **360**, pp. 601–622
[8] Kong S.Q., Song X.M., Sun Z.D., *ET AL.*: 'Well-aligned Au/TiO_2 nanorods arrays for the photodegradation of MB by magnetron sputtering', *Rare Metal Mat. Eng.*, 2018, **47**, pp. 1113–1118
[9] Jain N., Ravishankar N., Madras G.: 'Spectroscopic and kinetic insights of Pt-dispersion over microwave-synthesized GO-supported Pt-TiO_2 for CO oxidation', *Mol. Catal.*, 2017, **432**, pp. 88–98
[10] Su K.Y., Chen C.Y., Wu R.J.: 'Preparation of Pd/TiO_2 nanowires for the photoreduction of CO_2 into renewable hydrocarbon fuels', *J. Taiwan Inst. Chem. E*, 2019, **96**, pp. 409–418
[11] Hou W.B., Cronin S.B.: 'A review of surface plasmon resonance-enhanced photocatalysis', *Adv. Funct. Mater.*, 2012, **23**, pp. 1612–1619
[12] Liu X., Liu Z.Q., Lu J.L., *ET AL.*: 'Electrodeposition preparation of Ag nanoparticles loaded TiO_2 nanotube arrays with enhanced photocatalytic performance', *Appl. Surf. Sci.*, 2014, **288**, pp. 513–517
[13] Gomes J., Lopes A., Bednarczyk K., *ET AL.*: 'Environmental preservation of emerging parabens contamination: effect of Ag and Pt loading over the catalytic efficiency of TiO_2 during photocatalytic ozonation', *Energy Proc.*, 2017, **136**, pp. 270–276
[14] Elleuch L., Messaoud M., Djebali K., *ET AL.*: 'A new insight into highly contaminated landfill leachate treatment using Kefir grains pre-treatment combined with Ag-doped TiO_2 photocatalytic process', *J. Hazard. Mater.*, 2020, **382**, p. 121119
[15] Assaud L., Brazeau N., Barr M.K.S., *ET AL.*: 'Atomic layer deposition of Pd nanoparticles on TiO_2 nanotubes for ethanol electrooxidation: synthesis and electrochemical properties', *ACS Appl. Mater. Interfaces*, 2015, **7**, pp. 24533–24542
[16] Pelin Y., Armando M.L., Igor L., *ET AL.*: 'Photoelectrocatalysis of Rhodamine B and solar hydrogen production by TiO_2 and Pd/TiO_2 catalyst systems', *Electrochim. Acta*, 2017, **231**, pp. 641–649
[17] Singh J., Dutta T., Kim K.H., *ET AL.*: ''Green' synthesis of metals and their oxide nanoparticles: applications for environmental remediation', *J. Nanobiotechnol.*, 2019, **16**, pp. 84–107
[18] Singh J., Kumar V., Jolly S.S., *ET AL.*: 'Biogenic synthesis of silver nanoparticles and its photocatalytic applications for removal of organic pollutants in water', *J. Ind. Eng. Chem.*, 2019, **80**, pp. 247–257
[19] Singh K., Kukkar D., Singh R., *ET AL.*: 'In situ green synthesis of Au/Ag nanostructures on a metal-organic framework surface for photocatalytic reduction of p-nitrophenol', *J. Ind. Eng. Chem.*, 2020, **81**, pp. 196–205
[20] Kaur H., Kaur S., Singh J., *ET AL.*: 'Expanding horizon: green synthesis of TiO_2 nanoparticles using *Carica papaya* leaves for photocatalysis application', *Mater. Res. Express*, 2019, **6**, p.095034
[21] He Y.R., Cheng Y.Y., Wang W.K., *ET AL.*: 'A green approach to recover Au (III) in aqueous solution using biologically assembled rGO hydrogels', *Chem. Eng. J.*, 2015, **270**, pp. 476–484
[22] Xu H., Tan L., Cui H., *ET AL.*: 'Characterization of Pd(II) biosorption in aqueous solution by *Shewanella oneidensis* MR-1', *J. Mol. Liq.*, 2018, **255**, pp. 333–340
[23] Bao H., Zheng Z.W., Yang B., *ET AL.*: 'In situ monitoring of *Shewanella oneidensis* MR-1 biofilm growth on gold electrodes by using a Pt microelectrode', *Bioelectrochemistry*, 2016, **109**, pp. 95–100
[24] Xiao X., Liu Q.Y., Lu X.R., *ET AL.*: 'Self-assembly of complex hollow CuS nano/micro shell by an electrochemically active bacterium *Shewanella oneidensis* MR-1', *Int. Biodeter. Biodegr.*, 2017, **116**, pp. 10–16
[25] Xiao X., Zhu W.W., Yuan H., *ET AL.*: 'Biosynthesis of FeS nanoparticles from contaminant degradation in one single system', *Biochem. Eng. J.*, 2016, **105**, pp. 214–219
[26] Wiley B., Herricks T., Sun Y., *ET AL.*: 'Polyol synthesis of silver nanoparticles: use of chloride and oxygen to promote the formation of single-crystal, truncated cubes and tetrahedrons', *Nano Lett.*, 2004, **4**, pp. 1733–1739
[27] Wang D., Zhou Z.H., Yang H., *ET AL.*: 'Preparation of TiO_2 loaded with crystalline nano Ag by a one-step low-temperature hydrothermal method', *J. Mater. Chem.*, 2012, **22**, pp. 16306–16311
[28] Huang H., Leung D.Y.C.: 'Complete oxidation of formaldehyde at room temperature using TiO_2-supported metallic Pd nanoparticles', *ACS Catal.*, 2011, **1**, pp. 348–354
[29] Le F., Brandl D.W., Urzhumov Y.A.: 'Metallic nanoparticle arrays: a common substrate for both surface-enhanced Raman scattering and surface enhanced infrared absorption', *ACS Nano*, 2008, **2**, pp. 707–718
[30] Chen Q.H., Xin Y.J., Zhu X.W.: 'Au–Pd nanoparticles-decorated TiO_2 nanobelts for photocatalytic degradation of antibiotic levofloxacin in aqueous solution', *Electrochim. Acta*, 2015, **186**, pp. 34–42
[31] Khan M.M., Lee J., Cho M.H.: 'Au@TiO_2 nanocomposites for the catalytic degradation of methyl orange and methylene blue: an electron relay effect', *J. Ind. Eng. Chem.*, 2014, **20**, pp. 1584–1590
[32] Gupta N., Singh H.P., Sharma R.K.: 'Metal nanoparticles with high catalytic activity in degradation of methyl orange: an electron relay effect', *J. Mol. Catal. A, Chem.*, 2011, **335**, pp. 248–252
[33] Mallick K., Witcomb M.J., Scurrell M.S.: 'Redox catalytic property of gold nanoclusters: evidence of an electron-relay effect', *Appl. Phys. A, Mater. Sci. Process.*, 2005, **80**, pp. 797–801
[34] Yan F.F., He Y.R., Wu C., *ET AL.*: 'Carbon nanotubes alter the electron flow route and enhance nitrobenzene reduction by *Shewanella oneidensis* MR-1', *Environ. Sci. Technol. Lett.*, 2014, **1**, pp. 128–132
[35] Hau H.H., Gralnick J.A.: 'Ecology and biotechnology of the genus *Shewanella'*, *Annu. Rev. Microbiol.*, 2007, **61**, pp. 237–258